mathematics

Article

Hybrid Method for Inverse Elastic Obstacle Scattering Problems

Yuhan Yin * and Juan Liu

Department of Mathematics, Jinan University, Guangzhou 510632, China
* Correspondence: 2020y@stu2020.jnu.edu.cn

Abstract: The problem of determining the shape of an object from knowledge of the far-field of a single incident wave in two-dimensional elasticity was considered. We applied an iterative hybrid method to tackle this problem. An advantage of this method is that it does not need a forward solver, and therefore, the exact boundary condition is not essential. By deriving the Fréchet derivatives of two boundary operators, we established reconstruction algorithms for objects with Dirichlet, Neumann, and Robin boundary conditions; by introducing a general boundary condition, we also established the reconstruction algorithm for objects with unknown physical properties. Numerical experiments showed the effectiveness of the proposed method.

Keywords: inverse scattering; elastic wave; far-field; obstacle reconstruction; iterative method

MSC: 78A46; 65N21; 74J25

Citation: Yin, Y.; Liu, J. Hybrid Method for Inverse Elastic Obstacle Scattering Problems. *Mathematics* **2023**, *11*, 1939. https://doi.org/10.3390/math11081939

Academic Editor: Jürgen Frikel

Received: 24 February 2023
Revised: 7 April 2023
Accepted: 17 April 2023
Published: 20 April 2023

1. Introduction

The inverse obstacle problem of recovering the location and shape of a scattering object from knowledge of the far-field is a classic problem in inverse scattering [1]. Recently, inverse obstacle problems of a scattered time-harmonic elastic wave have received increased attention for their significant applications in many scientific areas, such as geophysics and seismology [2–8]. We refer to [9–12] for a comprehensive introduction of the mathematical theory of direct and inverse elastic scattering problems.

If far-field data for a large number of incident elastic plane waves are available, both the location and shape of the obstacle can be reconstructed by using the linear sampling method [13], the factorization method [14–16], or reverse time migration [17]. However, if only the far-field pattern due to a single incident wave is available, the reconstruction becomes severely ill-posed and, thus, more challenging [6]. There exist some sampling-type methods for inverse elastic obstacle scattering problems using one incident wave, e.g., the extended sampling method [18,19], the one-wave factorization method [4,20], and the direct sampling method [2]. The sampling methods do not need prior information on the physical and geometrical properties of the obstacle, but they can only reconstruct the location and size of the obstacle. To determine the shape of the obstacle, one must use iterative methods [8,21–24]. Iterative methods can recover the shape of the obstacle with a suitable initial approximation; they usually require forward solvers and, therefore, need the boundary condition of the obstacle. When the physical property of the obstacle is not available, iterative methods may fail.

In this paper, we considered inverse elastic obstacle scattering problems using the far-field pattern due to one incident wave. For the unique results on the inverse problems, we refer to [20,25] and the references therein. We are interested in an iterative method for inverse acoustic obstacle scattering problems introduced by Chapko, Kress, and Serranho [26–31]. This method combines ideas of both the decomposition method [32–34] and iterative Newton methods [35,36] and is, therefore, called a hybrid method. Since the hybrid method obtains good reconstructions from far-field data for a single incident wave and does not need a forward solver, it can be improved and used even when the boundary condition is not available [37]. In this work, we give a nontrivial extension of the hybrid method and its improved version in [28–31,37] for the inverse elastic scattering problems. The elastic wave equation is more challenging because of the coexistence of compressional waves and shear waves propagating at different speeds, and the boundary conditions of the obstacle for elastic waves are more complicated. Hence, sophisticated modification is required in our extension.

The paper is organized as follows. In Section 2, we introduce the direct elastic scattering problem and four inverse problems. We prove that a general boundary equation system is always satisfied on the exact boundary of the object. In Section 3, we give the Fréchet derivatives of five boundary operators, which are important for our iterative schemes. Section 4 is devoted to hybrid methods for four inverse problems. In Section 5, numerical experiments are given to demonstrate the effectiveness and promising features of the proposed numerical methods. Finally, in Section 6, we make some conclusions.

2. Direct and Inverse Scattering Problems

We begin with the notation used throughout this paper. For a non-zero vector $x \in \mathbb{R}^2$, let $\hat{x} := x/|x|$ and $\hat{x}^\perp$ be obtained by rotating $\hat{x}$ clockwise by $\pi/2$. For the vector function $u = (u_1; u_2)$, in addition to the usual differential operators $\operatorname{grad} u_j := (\partial_1 u_j; \partial_2 u_j), j = 1, 2$ and $\operatorname{div} u := \partial_1 u_1 + \partial_2 u_2$, we made use of $\operatorname{grad}^\perp u_j := (-\partial_2 u_j; \partial_1 u_j)$ and $\operatorname{div}^\perp u := \partial_1 u_2 - \partial_2 u_1$, where ∂_i denotes $\partial/\partial x_i, i = 1, 2$.

The propagation of time-harmonic waves in an isotropic homogeneous medium with Lamé constants λ and μ ($\mu > 0$, $2\mu + \lambda > 0$) and density ρ is governed by the Navier equation (or system):

$$\Delta^* u + \rho\omega^2 u = 0, \tag{1}$$

where u denotes the displacement field, ω denotes the angular frequency, and the differential operator $\Delta^* u := \mu\Delta u + (\lambda + \mu) \operatorname{grad} \operatorname{div} u$. In this paper, we assumed $\rho \equiv 1$. It is well known that any solution u of (1) can be decomposed as

$$u = u_p + u_s,$$

where

$$u_p := -\frac{1}{k_p^2} \operatorname{grad} \operatorname{div} u, \qquad u_s := -\frac{1}{k_s^2} \operatorname{grad}^\perp \operatorname{div}^\perp u \tag{2}$$

are known as the compressional part of u associated with the compressional wavenumber $k_p := \omega/\sqrt{2\mu + \lambda}$ and the shear part of u associated with the shear wavenumber $k_s := \omega/\sqrt{\mu}$, respectively.

The direct elastic scattering problem for an obstacle is as follows: Given a bounded domain D of class C^2 and an incident field u^{inc} such that u^{inc} is a solution of (1) in a neighborhood of ∂D and $u^{\text{inc}}|_{\partial D} \in [C(\partial D)]^2$, find the scattered field $u^{\text{sca}} \in [C^2(\mathbb{R}^2 \setminus \bar{D}) \bigcap C^1(\mathbb{R}^2 \setminus D)]^2$ and total field $u := u^{\text{sca}} + u^{\text{inc}}$ subject to

$$\begin{cases} \Delta^* u + \omega^2 u = 0, \quad \text{in } \mathbb{R}^2 \setminus \bar{D}, \\ B(u) = 0, \quad \text{on } \partial D, \\ \lim\limits_{r\to\infty} \sqrt{r}(\partial u_p^{\text{sca}}/\partial r - ik_p u_p^{\text{sca}}) = 0, \quad r = |x|, \\ \lim\limits_{r\to\infty} \sqrt{r}(\partial u_s^{\text{sca}}/\partial r - ik_s u_s^{\text{sca}}) = 0, \quad r = |x|. \end{cases} \tag{3}$$

The operator B in (3) defines the boundary condition on ∂D, which depends on the physical properties of the scatterer. The most-frequently occurring boundary conditions are as follows:

(1) The Dirichlet boundary condition:

$$u = 0 \quad \text{on } \partial D, \tag{4}$$

for a rigid body;

(2) The Neumann boundary condition:

$$T_\nu u = 0 \quad \text{on } \partial D, \tag{5}$$

for a cavity, where $T_\nu := 2\mu\frac{\partial}{\partial\nu} + \lambda\nu \operatorname{div} - \mu\nu^\perp \operatorname{div}^\perp$ denotes the surface traction operator and ν is the unit outward normal to ∂D;

(3) The Robin boundary condition:

$$T_\nu u + i\sigma u = 0 \quad \text{on } \partial D, \tag{6}$$

for an obstacle with some real-valued parameter $\sigma > 0$.

For the unique solvability of the scattering problem (3) in the space $[H^1_{loc}(\mathbb{R}^2 \setminus \bar{D})]^2$, we refer to [9,21].

It is well known that every radiation solution to the Navier equation has an asymptotic behavior of the form:

$$u^{\text{sca}}(x) = \frac{e^{ik_p|x|}}{\sqrt{|x|}} u_p^\infty(\hat{x})\hat{x} + \frac{e^{ik_s|x|}}{\sqrt{|x|}} u_s^\infty(\hat{x})\hat{x}^\perp + O(|x|^{-3/2}), \quad |x| \to \infty \tag{7}$$

uniformly in all directions $\hat{x}$, where u_p^∞ and u_s^∞ are analytic functions on the unit circle $S^2 := \{\hat{x} \in \mathbb{R}^2; |\hat{x}| = 1\}$. Throughout this paper, $u_\infty(\hat{x}) := (u_p^\infty(\hat{x}); u_s^\infty(\hat{x}))$ is defined as the far-field pattern of u^{sca}, and u_p^∞ and u_s^∞ are defined as the compressional part and shear part of the far-field pattern, respectively.

The inverse scattering problem of interest is to reconstruct the shape of the scatterer with the far-field pattern of all observation directions available, but only one single incident wave. In particular, four inverse elastic scattering problems are considered:

IP1. If the Dirichlet boundary condition is known to be satisfied on ∂D, determine the shape of the scatterer D from the far-field pattern $u_\infty(\hat{x}), \hat{x} \in S$ due to one incident wave.

IP2. If the Neumann boundary condition is known to be satisfied on ∂D, determine the shape of the scatterer D from the far-field pattern $u_\infty(\hat{x}), \hat{x} \in S$ due to one incident wave.

IP3. If the Robin boundary condition is known to be satisfied on ∂D, determine the shape of the scatterer D from the far-field pattern $u_\infty(\hat{x}), \hat{x} \in S$ due to one incident wave.

IP4. If the boundary condition on ∂D is unknown, determine the shape of the scatterer D from the far-field pattern $u_\infty(\hat{x}), \hat{x} \in S$ due to one incident wave.

For the inverse elastic scattering problems with a single incident wave, there are some uniqueness results proven within polygonal, polyhedral, or ball scatterers, and establishing the general uniqueness results still remains challenging open problem (see [15,20,25]).

When the boundary condition is unknown, the following theorem is crucial for the numerical solution of IP4.

Theorem 1. *The total field $u = (u_1; u_2)$ satisfies $u = 0$, $T_\nu u = 0$, or $T_\nu u + i\sigma u = 0$ for any $x \in \partial D$ if and only if u satisfies*

$$\begin{cases} \Re(T_\nu u).*\Re(u) + \Im(T_\nu u).*\Im(u) = 0 \\ \Re(T_\nu u).*\Re(u)^\perp + \Im(T_\nu u)^\perp.*\Im(u) = 0 \\ \Re(T_\nu u).*\Im(u)^\perp - \Re(T_\nu u)^\perp.*\Im(u) = 0 \\ \Im(T_\nu u).*\Re(u)^\perp - \Im(T_\nu u)^\perp.*\Re(u) = 0 \end{cases} \tag{8}$$

for $x \in \partial D$, where $\Re(A)$ and $\Im(A)$ denote the real and imaginary parts of vector A, respectively, and $A. * B$ denotes the elementwise product of vectors A and B.

Proof. For any point $x \in \partial D$, if $u = 0$ or $T_\nu u = 0$ at x, it is apparent that u satisfies (8) at x. If $T_\nu u + i\sigma u = 0$ at x, by taking the real part and the imaginary part of this equation, we have

$$\Re(T_\nu u) = \sigma \Im(u),$$
$$\Im(T_\nu u) = -\sigma \Re(u),$$

which imply

$$\Re(T_\nu u)^\perp = \sigma \Im(u)^\perp,$$
$$\Im(T_\nu u)^\perp = -\sigma \Re(u)^\perp,$$

and we can easily obtain (8) from the above four equations.

On the other hand, if (8) is satisfied on ∂D, then

$$\begin{aligned} & u. * \Re(T_\nu u) - i\Im(u). * T_\nu u \\ = & \Big[\Re(u) + i\Im(u)\Big]. * \Re(T_\nu u) - i\Im(u). * \Big[\Re(T_\nu u) + i\Im(T_\nu u)\Big] \\ = & \Re(T_\nu u). * \Re(u) + \Im(T_\nu u). * \Im(u) \\ = & 0. \end{aligned} \tag{9}$$

Similarly, we can deduce

$$u. * \Im(T_\nu u) + i\Re(u). * T_\nu u = 0, \tag{10}$$

$$u. * \Re(T_\nu u)^\perp - i\Im(u)^\perp. * T_\nu u = 0, \tag{11}$$

$$u. * \Im(T_\nu u)^\perp + i\Re(u)^\perp. * T_\nu u = 0. \tag{12}$$

Taking the elementwise products of (9)–(12) with $i\Im(u), -i\Re(u), i\Im(u)^\perp, -i\Re(u)^\perp$ and then taking the sum of these four equations, we obtain

$$\begin{aligned} & \Big[\Im(u). * \Im(u) + \Re(u). * \Re(u) + \Im(u)^\perp. * \Im(u)^\perp + \Re(u)^\perp. * \Re(u)^\perp\Big]. * T_\nu u \\ & + iu. * \Big[\Re(T_\nu u). * \Im(u) - \Im(T_\nu u). * \Re(u) + \Re(T_\nu u)^\perp. * \Im(u)^\perp - \Im(T_\nu u)^\perp \\ & . * \Re(u)^\perp\Big] = 0 \quad \text{on } \partial D. \end{aligned}$$

The above equation implies that $u = 0$, or $T_\nu u + i\sigma u = 0$ at any point $x \in \partial D$, where

$$\sigma(x) = \frac{\Re(w_1)\Im(u_1) + \Re(w_2)\Im(u_2) - \Im(w_1)\Re(u_1) - \Im(w_2)\Re(u_2)}{\big(\Re(u_1)\big)^2 + \big(\Im(u_1)\big)^2 + \big(\Re(u_2)\big)^2 + \big(\Im(u_2)\big)^2}.$$

Here, w_1 and w_2 denote the two components of $w := T_\nu u$. □

Remark 1. *From Theorem 1, if the total field of the elastic scattering problem satisfies the Dirichlet, Neumann, or Robin boundary condition on ∂D, it must satisfy the general boundary condition (8) on ∂D.*

3. Fréchet Derivatives of Five Boundary Operators

In this section, let Γ be any closed C^2-contour, let v be a C^1 smooth scalar function in the space near Γ, and assume that boundary Γ has a parametric form:

$$\Gamma = \{z(t) : t \in [0, 2\pi]\}$$

with $z(t) \in C^2[0,2\pi] \times C^2[0,2\pi]$.

The operators that we will consider include the normal operator $\nu : C^2[0,2\pi] \times C^2[0,2\pi] \to C[0,2\pi] \times C[0,2\pi]$:

$$\nu : z \mapsto \frac{z'^{\perp}}{|z'|}, \tag{13}$$

the tangential operator $\tau : C^2[0,2\pi] \times C^2[0,2\pi] \to C[0,2\pi] \times C[0,2\pi]$:

$$\tau : z \mapsto \frac{z'}{|z'|}, \tag{14}$$

the Dirichlet operator $B_{D,v} : C^2[0,2\pi] \times C^2[0,2\pi] \to C[0,2\pi]$ that maps the parameterization z of the contour Γ to the exterior trace of v over Γ, that is

$$B_{D,v} : z \mapsto v \circ z, \tag{15}$$

the normal derivative operator $B_{N,v} : C^2[0,2\pi] \times C^2[0,2\pi] \to C[0,2\pi]$ that maps the parameterization z of the contour Γ to the exterior trace of $\partial v/\partial \nu$ over Γ, that is

$$B_{N,v} : z \mapsto \frac{\partial v}{\partial \nu} \circ z, \tag{16}$$

and the tangential derivative operator $B_{T,v} : C^2[0,2\pi] \times C^2[0,2\pi] \to C[0,2\pi]$ that maps the parameterization z of the contour Γ to the exterior trace of the $\partial v/\partial \tau$ over Γ, that is

$$B_{T,v} : z \mapsto \frac{\partial v}{\partial \tau} \circ z. \tag{17}$$

The Fréchet derivatives of the Dirichlet operator, normal operator, and normal derivative operator were considered in [28,31].

Theorem 2 ([31])**.** *The Dirichlet operator $B_{D,v}$ defined in* (15) *is Fréchet differentiable, and the Frećhet derivative is given by*

$$B'_{D,v}(z)h = (\nu \cdot h)\frac{\partial v}{\partial \nu} \circ z + (\tau \cdot h)\frac{\partial v}{\partial \tau} \circ z. \tag{18}$$

Theorem 3 ([31])**.** *The normal operator ν defined in* (13) *is Fréchet differentiable, and its Fréchet derivative is given by*

$$\nu'(z)h = -\frac{1}{|z'|}(h' \cdot \nu)\tau. \tag{19}$$

Theorem 4 ([28])**.** *The operator $B_{N,v}$ defined in* (16) *is Fréchet differentiable, and the Fréchet derivative is given by*

$$B'_{N,v}(z)h = -\frac{(h' \cdot \nu)}{|z'|}\frac{\partial v}{\partial \tau} \circ z + (h \cdot \tau)\left[\frac{\partial^2 v}{\partial \tau \partial \nu} \circ z - H\frac{\partial v}{\partial \tau} \circ z\right] + (h \cdot \nu)\frac{\partial^2 v}{\partial \nu^2}, \tag{20}$$

where $H = -(z'' \cdot \nu)/|z'|^2$.

In the following, we characterize the Fréchet derivatives of the tangential operator and the tangential derivative operator.

Theorem 5. *The tangential operator τ defined in* (14) *is Fréchet differentiable. The Fréchet derivative is given by*

$$\tau'(z)h = \frac{1}{|z'|}(h' \cdot \nu)\nu. \tag{21}$$

Proof. Since $\tau(z) = \frac{z'}{|z'|}$, we have

$$\tau(z+h) - \tau(z) = \frac{z'+h'}{|z'+h'|} - \frac{z'}{|z'|}.$$

From Taylor's formula,

$$\begin{aligned}
\frac{z'+h'}{|z'+h'|} - \frac{z'}{|z'|} &= \frac{1}{|z'|^3}\begin{bmatrix} z_2'^2 h_1' - z_1' z_2' h_2' \\ -z_1' z_2' h_1' + z_1'^2 h_2' \end{bmatrix} + O(|h'|^2) \\
&= \frac{1}{|z'|^3}\Big[|z'|^2 h' - z'(z' \cdot h')\Big] + O(|h'|^2) \\
&= \frac{1}{|z'|}\left[h' - (h' \cdot \tau)\tau\right] + O(|h'|^2) \\
&= \frac{1}{|z'|}(h' \cdot \nu)\nu + O(|h'|^2)
\end{aligned}$$

These two equations imply

$$\lim_{\|h\|_{C^2} \to 0} \frac{\|\tau(z+h) - \tau(z) - \frac{1}{|z'|}(h' \cdot \nu)\nu\|_\infty}{\|h\|_{C^2}} = 0.$$

One can obtain the derivative of $\tau(z)$ by the definition of the Fréchet derivative. □

Theorem 6. *The operator $B_{T,v}$ defined in (17) is Frećhet differentiable, and the Fréchet derivative is given by*

$$\begin{aligned}
B'_{T,v}(z)h =& \frac{(h' \cdot \nu)}{|z'|}\frac{\partial v}{\partial \nu} \circ z + (h \cdot \tau)\left[H\frac{\partial v}{\partial \nu} \circ z + \frac{\partial^2 v}{\partial \tau^2} \circ z\right] \\
&+ (h \cdot \nu)\left[\frac{\partial^2 v}{\partial \tau \partial \nu} \circ z - H\frac{\partial v}{\partial \tau} \circ z\right],
\end{aligned} \tag{22}$$

where $H = -(z'' \cdot \nu)/|z'|^2$.

Proof. Let h be sufficiently small to ensure that

$$\Gamma_{z+h} = \{z(t) + h(t) : t \in [0, 2\pi]\}$$

describes a closed curve.

We divided $B_{T,v}(z+h) - B_{T,v}(z)$ into two parts:

$$\begin{aligned}
B_{T,v}(z+h) - B_{T,v}(z) =& (\tau \cdot \mathrm{grad}\, v) \circ (z+h) - (\tau \cdot \mathrm{grad}\, v) \circ z \\
=& \frac{z'+h'}{|z'+h'|} \cdot \mathrm{grad}\, v \circ (z+h) - \frac{z'}{|z'|} \cdot \mathrm{grad}\, v \circ z \\
=& \left(\frac{z'+h'}{|z'+h'|} - \frac{z'}{|z'|}\right) \cdot \mathrm{grad}\, v \circ (z+h) \\
&+ \frac{z'}{|z'|}\Big(\mathrm{grad}\, v \circ (z+h) - \mathrm{grad}\, v \circ z\Big).
\end{aligned} \tag{23}$$

For the first term on the right side of (23), by using Taylor's formula, we have

$$\mathrm{grad}\, v \circ (z+h) - \mathrm{grad}\, v \circ (z) = O(|h|),$$

and

$$\frac{z'+h'}{|z'+h'|} - \frac{z'}{|z'|} = \frac{1}{|z'|}(h' \cdot \nu)\nu + O(|h'|^2).$$

These two equations imply

$$\left(\frac{z'+h'}{|z'+h'|}-\frac{z'}{|z'|}\right)\cdot \operatorname{grad} v\circ(z+h)=\frac{(h'\cdot\nu)}{|z'|}\frac{\partial v}{\partial\nu}+\mathrm{O}(|h'|^2)+\mathrm{O}(|h'||h|). \tag{24}$$

Now, we considered the second term on the right side of (23). A new coordinate system (t,ε) is introduced (see [31,38]). The relation between the new system and the Cartesian coordinate system is

$$x(t,\varepsilon)=z(t)+\varepsilon\nu(t),\quad t\in[0,2\pi],\ \varepsilon\in(-\varepsilon_0,\varepsilon_0),$$

where $\nu(t)$ is the abbreviation of $\nu(z(t))$. In this new coordinate system, the gradient of v can be rewritten as (see [31,38])

$$\operatorname{grad} v(t,\varepsilon)=\frac{1}{|z'(t)+\varepsilon\nu'(t)|^2}\frac{\partial v}{\partial t}(t,\varepsilon)\left[z'(t)+\varepsilon\nu'(t)\right]+\frac{\partial v}{\partial\varepsilon}(t,\varepsilon)\nu(t). \tag{25}$$

If we let $\sigma=(h\cdot\tau)/|z'|$ and $\epsilon=h\cdot\nu$, then

$$\begin{aligned}
z(t)+h(t) &= z(t)+\big(h(t)\cdot\tau(t)\big)\tau(t)+\big(h(t)\cdot\nu(t)\big)\nu(t)\\
&= z(t)+\sigma z'(t)+\epsilon\nu(t)\\
&= z(t+\sigma)+\epsilon\nu(t+\sigma)+\mathrm{O}(|h|^2).
\end{aligned} \tag{26}$$

Using (25) and (26), together with Taylor's formula, we have

$$\begin{aligned}
&\operatorname{grad} v\circ(z+h)-\operatorname{grad} v\circ z\\
=\ &\operatorname{grad} v\circ\left[z(t+\sigma)+\epsilon\nu(t+\sigma)+\mathrm{O}(|h|^2)\right]-\operatorname{grad} v\circ\left[z(t)\right]\\
=\ &\operatorname{grad} v\circ\left[z(t+\sigma)+\epsilon\nu(t+\sigma)\right]-\operatorname{grad} v\circ\left[z(t)\right]+\mathrm{O}(|h|^2)\\
=\ &\operatorname{grad} v(t+\sigma,\epsilon)-\operatorname{grad} v(t,0)+\mathrm{O}(|h|^2)\\
=\ &\frac{z'(t+\sigma)+\epsilon\nu'(t+\sigma)}{|z'(t+\sigma)+\epsilon\nu'(t+\sigma)|^2}\frac{\partial v}{\partial t}(t+\sigma,\epsilon)+\frac{\partial v}{\partial\varepsilon}(t+\sigma,\epsilon)\nu(t+\sigma)\\
&-\frac{z'(t)}{|z'(t)|^2}\frac{\partial v}{\partial t}(t,0)-\frac{\partial v}{\partial\varepsilon}(t,0)\nu(t)\\
=\ &\left[\frac{z'(t+\sigma)+\epsilon\nu'(t+\sigma)}{|z'(t+\sigma)+\epsilon\nu'(t+\sigma)|^2}-\frac{z'(t)}{|z'(t)|^2}\right]\frac{\partial v}{\partial t}(t+\sigma,\epsilon)\\
&+\frac{z'(t)}{|z'(t)|^2}\left[\frac{\partial v}{\partial t}(t+\sigma,\epsilon)-\frac{\partial v}{\partial t}(t,0)\right]\\
&+\left[\frac{\partial v}{\partial\varepsilon}(t+\sigma,\epsilon)-\frac{\partial v}{\partial\varepsilon}(t,0)\right]\nu(t+\sigma)+\left[\nu(t+\sigma)-\nu(t)\right]\frac{\partial v}{\partial\varepsilon}(t,0)\\
=\ &\frac{1}{|z'|^2}\left[\sigma(z''\cdot\nu)\nu-\sigma(z''\cdot\tau)\tau-\epsilon(\nu'\cdot\tau)\tau\right]\frac{\partial v}{\partial t}(t,0)\\
&+\frac{\tau}{|z'|}\left[\epsilon\frac{\partial^2 v}{\partial t\partial\varepsilon}(t,0)+\sigma\frac{\partial^2 v}{\partial t^2}(t,0)\right]+\nu'\sigma\frac{\partial v}{\partial\varepsilon}(t,0)\\
&+\nu\left[\sigma\frac{\partial^2 v}{\partial t\partial\varepsilon}(t,0)+\epsilon\frac{\partial^2 v}{\partial\varepsilon^2}(t,0)\right]+\mathrm{O}(|h|^2).
\end{aligned} \tag{27}$$

Therefore, with (27), $\sigma=(h\cdot\tau)/|z'|$, and $\epsilon=h\cdot\nu$, we have

$$
\begin{aligned}
& \tau \cdot \Big(\mathrm{grad} v \circ (z+h) - \mathrm{grad} v \circ z \Big) \\
= \;& -\frac{1}{|z'|^2}\Big[\sigma(z''\cdot\tau) + \epsilon(\nu'\cdot\tau)\Big]\frac{\partial v}{\partial t}(t,0) + \frac{1}{|z'|}\Big[\epsilon\frac{\partial^2 v}{\partial t\partial\varepsilon}(t,0) + \sigma\frac{\partial^2 v}{\partial t^2}(t,0)\Big] \\
& +\sigma(\nu'\cdot\tau)\frac{\partial v}{\partial\varepsilon}(t,0) + \mathrm{O}(|h|^2) \\
= \;& -\Big[\frac{(h\cdot\tau)}{|z'|^3}(z''\cdot\tau) + \frac{(h\cdot\nu)}{|z'|^2}(\nu'\cdot\tau)\Big]\frac{\partial v}{\partial t}(t,0) + \Big[\frac{(h\cdot\nu)}{|z'|}\frac{\partial^2 v}{\partial t\partial\varepsilon}(t,0) + \frac{(h\cdot\tau)}{|z'|^2}\frac{\partial^2 v}{\partial t^2}(t,0)\Big] \\
& +\frac{(h\cdot\tau)}{|z'|}(\nu'\cdot\tau)\frac{\partial v}{\partial\varepsilon}(t,0) + \mathrm{O}(|h|^2).
\end{aligned} \tag{28}
$$

To simplify (28), we use the relations

$$\nu'\cdot\tau = -\frac{1}{|z'|}(\nu\cdot z''), \tag{29}$$

$$\frac{\partial v}{\partial\varepsilon}(t,0) = \big[\mathrm{grad}\; v(t,0)\big]\cdot\nu(t) = \frac{\partial v}{\partial\nu}\circ z, \tag{30}$$

$$\frac{1}{|z'(t)|}\frac{\partial v}{\partial t}(t,0) = \big[\mathrm{grad}\; v(t,0)\big]\cdot\tau(t) = \frac{\partial v}{\partial\tau}\circ z, \tag{31}$$

$$\frac{1}{|z'(t)|^2}\frac{\partial^2 v}{\partial t^2}(t,0) = \frac{\partial^2 v}{\partial\tau^2}\circ z + \frac{(\tau\cdot z'')}{|z'|^2}\frac{\partial v}{\partial\tau}\circ z, \tag{32}$$

$$\frac{1}{|z'(t)|}\frac{\partial^2 v}{\partial\varepsilon\partial t}(t,0) = \frac{\partial^2 v}{\partial\tau\partial\nu}\circ z, \tag{33}$$

where (29) is obtained by direct computation, (30) and (31) are obtained from (25), and the relations (32) and (33) are obtained by replacing v with $\frac{\partial v}{\partial t}$ in (30) and (31). With the relations (29)–(33) and (28), we can write the second term on the right side of (23) as

$$
\begin{aligned}
\tau\cdot\Big(\mathrm{grad} u\circ(z+h) - \mathrm{grad} u\circ z\Big) = & -(h\cdot\nu)H\frac{\partial u}{\partial\tau}\circ z + (h\cdot\nu)\frac{\partial^2 u}{\partial\tau\partial\nu}\circ z \\
& + (h\cdot\tau)\frac{\partial^2 u}{\partial\tau^2}\circ z + (h\cdot\tau)H\frac{\partial u}{\partial\nu}\circ z + \mathrm{O}(|h|^2),
\end{aligned} \tag{34}
$$

where $H := -(z''\cdot\nu)/|z'|^2$.

Inserting (24) and (34) into (23), one can obtain the expression of the Fréchet derivative of $B_{T,v}$ from the definition of the Fréchet derivative. □

4. Hybrid Method

In this section, we propose a hybrid method to reconstruct the shape of the scatterer ∂D from the far-field pattern $u^\infty(\hat{x}) = (u_p^\infty(\hat{x}), u_s^\infty(\hat{x}))$, $\hat{x}\in\mathbb{S}^2$ of the elastic scattering problem (3); more specifically, we solve the four inverse problems IP1, IP2, IP3, and IP4.

4.1. Basic Algorithm of the Hybrid Method

The hybrid method consists of two steps in the same spirit as a decomposition method, which are iterated until some stopping criterion is achieved as in an iterative method. We denote the approximation at the nth iteration to the exact boundary ∂D by a closed C^2-contour Γ_n and suppose that Γ_n can be parameterized by a C^2-smooth function $z_n(t)$, $t\in[0,2\pi]$.

In the first step, we compute the total field u, its normal derivative $\frac{\partial u}{\partial \nu}$, and its tangential derivative $\frac{\partial u}{\partial \tau}$ on Γ_n from the far-field pattern $u_\infty(\hat{x}) := (u_p^\infty(\hat{x}); u_s^\infty(\hat{x})), \hat{x} \in S$. The fundamental solution tensor to the Navier equation (1) is (see [39])

$$\Phi(x,y) := \frac{i}{4\pi} H_0^{(1)}(k_s|x-y|)I + \frac{i}{4\omega^2} \mathrm{grad}_x \mathrm{grad}_x^T \left[H_0^{(1)}(k_s|x-y|) - H_0^{(1)}(k_p|x-y|) \right]$$

in terms of the identity matrix, I, and the Hankel function of the first kind of order zero, $H_0^{(1)}$. Using the Bessel differential equation, straightforward computations yield a representation of the form

$$\Phi(x,y) = \Phi_1(|x-y|)I + \Phi_2(|x-y|)J(|x-y|),$$

where, for $w \in \mathbb{R}^2 \setminus \{0\}$, the matrix J is given by

$$J(w) = \frac{ww^T}{|w|^2},$$

and where, for $r > 0$, the functions Φ_1 and Φ_2 are given by

$$\Phi_1(r) = \frac{i}{4\mu} H_0^{(1)}(k_s r) - \frac{i}{4\omega^2 r} \left[k_s H_1^{(1)}(k_s r) - k_p H_1^{(1)}(k_p r) \right],$$
$$\Phi_2(r) = \frac{i}{4\omega^2} \left[\frac{2k_s}{r} H_1^{(1)}(k_s r) - k_s^2 H_0^{(1)}(k_s r) - \frac{2k_p}{r} H_1^{(1)}(k_p r) + k_p^2 H_0^{(1)}(k_p r) \right],$$

with the Hankel function of the first kind of order one $H_1^{(1)} = -H_0^{(1)'}$. Then, choose $\tilde{\Gamma}_n$ to be a closed curve inside and near Γ_n and seek the scattered field u^{sca} in the form of an elastic single-layer potential over $\tilde{\Gamma}_n$ [39]:

$$u^{\mathrm{sca}}(x) = \int_{\tilde{\Gamma}_n} \Phi(x,y)\varphi(y)ds(y), \quad x \in \mathbb{R}^2 \setminus \tilde{\Gamma}_n. \tag{35}$$

From the asymptotics for Hankel functions, it follows that the far-field patterns of the above single-layer potential are given by

$$u_p^\infty(\hat{x}) = \frac{1}{\lambda + 2\mu} \frac{e^{i\pi/4}}{\sqrt{8\pi k_p}} \int_{\tilde{\Gamma}_n} (\hat{x} \cdot \varphi(y)) e^{-ik_p \hat{x} \cdot y} ds(y), \quad \hat{x} \in S, \tag{36}$$

$$u_s^\infty(\hat{x}) = \frac{1}{\mu} \frac{e^{i\pi/4}}{\sqrt{8\pi k_s}} \int_{\tilde{\Gamma}_n} (\hat{x}^\perp \cdot \varphi(y)) e^{-ik_s \hat{x} \cdot y} ds(y), \quad \hat{x} \in S. \tag{37}$$

In the experiments, the density function φ can be numerically solved from (36) and (37) using the Nyström method and the Tikhonov regularization method. Then, the scattered field u^{sca}, its normal derivative $\frac{\partial u^{\mathrm{sca}}}{\partial \nu}$, and its tangential derivative $\frac{\partial u^{\mathrm{sca}}}{\partial \tau}$ on Γ_n can be solved from (35). Since the incident waves are known, the total field u and its normal derivative $\frac{\partial u}{\partial \nu}$ and tangential derivative $\frac{\partial u}{\partial \tau}$ on Γ_n can be reconstructed.

In the second step, we solved for the improved approximation Γ_{n+1} from Γ_n. Suppose the total field u satisfies the boundary condition $B(u) = 0$ on the exact boundary ∂D. We considered the boundary operator $G : C^2[0,2\pi] \times C^2[0,2\pi] \to C[0,2\pi] \times C[0,2\pi]$ that maps a closed contour Γ with parameterization z onto the trace of the boundary condition of the total field u on Γ, that is

$$G : z \mapsto B(u) \circ z. \tag{38}$$

Apparently, if the parameterization of ∂D is z^*, then

$$G(z^*) = 0.$$

In the spirit of Newton's method, we linearized this equation based on the Fréchet derivative of G and solved

$$G(z_n) + G'(z_n)h = 0 \tag{39}$$

to obtain the shift h and a new approximation Γ_{n+1} to ∂D given by $z_{n+1} = z_n + h$. We summarize the basic algorithm as follows:

Basic algorithm:

1. Start with an initial guess $\Gamma_0 := \{z_0(t), t \in [0, 2\pi]\}$ of the exact boundary ∂D.
2. Solve for the total field u, its normal derivative $\frac{\partial u}{\partial \nu}$, and its tangential derivative $\frac{\partial u}{\partial \tau}$ on the approximation boundary $\Gamma_n := \{z_n(t), t \in [0, 2\pi]\}$:
    a. Use Tikhonov regularization to compute $\varphi(y), y \in \tilde{\Gamma}_n$ from the discrete version of (36) and (37), where $\tilde{\Gamma}_n$ is a closed curve inside and near Γ_n.
    b. Compute the scattered field u^{sca}, its normal derivative $\frac{\partial u^{\text{sca}}}{\partial \nu}$, and its tangential derivative $\frac{\partial u^{\text{sca}}}{\partial \tau}$ on Γ_n from (35).
    c. Estimate the total field u, its normal derivative $\frac{\partial u}{\partial \nu}$, and its tangential derivative $\frac{\partial u}{\partial \tau}$ on Γ_n.
3. Solve for the shift $h(t)$ from the linearized Equation (39) (the linearized equations for different inverse problems are particularized in Section 4.2), and then, update the approximation with Γ_{n+1} given by $z_{n+1} = z_n + h$.
4. Repeat Steps 2 and 3 with $n = n + 1$ until $\|G(z_{n+1})\|_{L^2} > \|G(z_n)\|_{L^2}$.

4.2. Linearized Equations for Different Inverse Problems

Once the expression of the linearized Equation (39) is given, the hybrid method can be iteratively implemented by following the basic algorithm above. Because the linearized Equation (39) is based on the boundary condition, which has different forms for different inverse problems, we need to particularize the linearized equation for each of these inverse problems.

4.2.1. Linearized Equation for IP1

For the inverse problem IP1, we denote the linearized equation by

$$G_D(z) + G'_D(z)h = 0 \tag{40}$$

for any approximation Γ to ∂D with parameterization $\Gamma := \{z(t), t \in [0, 2\pi]\}$.

Since the Dirichlet boundary condition $u = 0$ is satisfied on the exact boundary ∂D, from the definition of G in (38), the boundary operator for IP1 is

$$G_D(z) = u \circ z, \tag{41}$$

where u is considered to be a vector, that is

$$G_D(z) = \begin{bmatrix} u_1 \circ z \\ u_2 \circ z \end{bmatrix}. \tag{42}$$

According to Theorem 2, we have the Fréchet derivative of G_D:

$$G'_D(z)h = \begin{bmatrix} (\nu \cdot h)\frac{\partial u_1}{\partial \nu} \circ z + (\tau \cdot h)\frac{\partial u_1}{\partial \tau} \circ z \\ (\nu \cdot h)\frac{\partial u_2}{\partial \nu} \circ z + (\tau \cdot h)\frac{\partial u_2}{\partial \tau} \circ z \end{bmatrix}. \tag{43}$$

Therefore, the linearized equation for IP1 is (40), where $G_D(z)$ and $G'_D(z)h$ are defined in (42) and (43), respectively.

4.2.2. Linearized Equation for IP2

For the inverse problem IP2, we denote the linearized equation by

$$G_N(z) + G'_N(z)h = 0 \tag{44}$$

for any approximation Γ to ∂D with parameterization $\Gamma := \{z(t), t \in [0, 2\pi]\}$.

Since the total field u satisfies the Neumann boundary condition

$$T_\nu u := 2\mu \frac{\partial u}{\partial \nu} + \lambda \nu \text{ div } u + \mu \tau \text{ div}^\perp u = 0$$

on the exact boundary ∂D, from the definition of G in (38), the boundary operator for IP2 is

$$G_N(z) = 2\mu \frac{\partial u}{\partial \nu} \circ z + \lambda(\nu \text{ div } u) \circ z + \mu(\tau \text{ div}^\perp u) \circ z, \tag{45}$$

where $\nu = (\nu_1; \nu_2)$ and $\tau = (\tau_1; \tau_2)$ are normal and tangential vectors on Γ and

$$\begin{aligned} \text{div } u &= \frac{\partial u_1}{\partial x_1} + \frac{\partial u_2}{\partial x_2} \\ &= \nu_1 \frac{\partial u_1}{\partial \nu} + \tau_1 \frac{\partial u_1}{\partial \tau} + \nu_2 \frac{\partial u_2}{\partial \nu} + \tau_2 \frac{\partial u_2}{\partial \tau}, \end{aligned}$$

$$\begin{aligned} \text{div}^\perp u &= \frac{\partial u_2}{\partial x_1} - \frac{\partial u_1}{\partial x_2} \\ &= \nu_1 \frac{\partial u_2}{\partial \nu} + \tau_1 \frac{\partial u_2}{\partial \tau} - \nu_2 \frac{\partial u_1}{\partial \nu} - \tau_2 \frac{\partial u_1}{\partial \tau}. \end{aligned}$$

Since u, ν, and τ are all vectors, we can rewrite (45) by

$$G_N(z) = 2\mu \begin{bmatrix} \frac{\partial u_1}{\partial \nu} \circ z \\ \frac{\partial u_2}{\partial \nu} \circ z \end{bmatrix} + \lambda(\text{div } u \circ z) \begin{bmatrix} \nu_1(z) \\ \nu_2(z) \end{bmatrix} + \mu(\text{div}^\perp u \circ z) \begin{bmatrix} \tau_1(z) \\ \tau_2(z) \end{bmatrix}. \tag{46}$$

Now let us consider the Fréchet derivative of G_N. According to Theorem 3 and Theorem 5, we have the Fréchet derivatives $\nu'(z)h$ and $\tau'(z)h$ of operators $\nu(z)$ and $\tau(z)$, which imply the expressions of the Fréchet derivatives of the components $\nu_1(z)$, $\nu_2(z)$, $\tau_1(z)$, and $\tau_2(z)$:

$$\nu'_j(z)h = -\frac{(h' \cdot \nu)}{|z'|} \tau_j, \quad \tau'_j(z)h = \frac{(h' \cdot \nu)}{|z'|} \nu_j, \quad j = 1, 2.$$

For the operators $B_{N,u_1} : z \mapsto \frac{\partial u_1}{\partial \nu} \circ z$ and $B_{N,u_2} : z \mapsto \frac{\partial u_2}{\partial \nu} \circ z$, from Theorem 4, the Fréchet derivatives are

$$\begin{aligned} B'_{N,u_j}(z)h &= -\frac{(h' \cdot \nu)}{|z'|} \frac{\partial u_j}{\partial \tau} \circ z + (h \cdot \tau) \left[\frac{\partial^2 u_j}{\partial \tau \partial \nu} \circ z - H \frac{\partial u_j}{\partial \tau} \circ z \right] \\ &\quad + (h \cdot \nu) \frac{\partial^2 u_j}{\partial \nu^2} \circ z, \quad j = 1, 2, \end{aligned}$$

For the operators $B_{T,u_1} : z \mapsto \frac{\partial u_1}{\partial \tau} \circ z$ and $B_{T,u_2} : z \mapsto \frac{\partial u_2}{\partial \tau} \circ z$, from Theorem 6, the Fréchet derivatives have the expression

$$\begin{aligned} B'_{T,u_j}(z)h &= \frac{(h' \cdot \nu)}{|z'|} \frac{\partial u_j}{\partial \nu} \circ z + (h \cdot \tau) \left[H \frac{\partial u_j}{\partial \nu} \circ z + \frac{\partial^2 u_j}{\partial \tau^2} \circ z \right] \\ &\quad + (h \cdot \nu) \left[\frac{\partial^2 u_j}{\partial \tau \partial \nu} \circ z - H \frac{\partial u_j}{\partial \tau} \circ z \right], \quad j = 1, 2. \end{aligned}$$

Then, by using the product rule, we have the Fréchet derivative of $G_N(z)$, which is

$$\begin{aligned} G_N'(z)h &= 2\mu\begin{bmatrix} B'_{N,u_1}(z)h \\ B'_{N,u_2}(z)h \end{bmatrix} + \lambda(\mathrm{div}\, u\circ z)'\begin{bmatrix} \nu_1(z) \\ \nu_2(z) \end{bmatrix} - \lambda\frac{(h'\cdot\nu)}{|z'|}(\mathrm{div}\, u\circ z)\begin{bmatrix} \tau_1(z) \\ \tau_2(z) \end{bmatrix} \\ &\quad +\mu(\mathrm{div}^{\perp} u\circ z)'\begin{bmatrix} \tau_1(z) \\ \tau_2(z) \end{bmatrix} + \mu\frac{(h'\cdot\nu)}{|z'|}(\mathrm{div}^{\perp} u\circ z)\begin{bmatrix} \nu_1(z) \\ \nu_2(z) \end{bmatrix}, \end{aligned} \tag{47}$$

where

$$\begin{aligned} \left[\mathrm{div}\, u\circ z\right]' &= \left[\nu_1'(z)h\right]\frac{\partial u_1}{\partial\nu}\circ z + \nu_1(z)\left[B'_{N,u_1}(z)h\right] \\ &\quad +\left[\tau_1'(z)h\right]\frac{\partial u_1}{\partial\tau}\circ z + \tau_1(z)\left[B'_{T,u_1}(z)h\right] \\ &\quad +\left[\nu_2'(z)h\right]\frac{\partial u_2}{\partial\nu}\circ z + \nu_2(z)\left[B'_{N,u_2}(z)h\right] \\ &\quad +\left[\tau_2'(z)h\right]\frac{\partial u_2}{\partial\tau}\circ z + \tau_2(z)\left[B'_{T,u_2}(z)h\right] \end{aligned}$$

and

$$\begin{aligned} \left[\mathrm{div}^{\perp} u\circ z\right]' &= \left[\nu_1'(z)h\right]\frac{\partial u_2}{\partial\nu}\circ z + \nu_1(z)\left[B'_{N,u_2}(z)h\right] \\ &\quad +\left[\tau_1'(z)h\right]\frac{\partial u_2}{\partial\tau}\circ z + \tau_1(z)\left[B'_{T,u_2}(z)h\right] \\ &\quad -\left[\nu_2'(z)h\right]\frac{\partial u_1}{\partial\nu}\circ z - \nu_2(z)\left[B'_{N,u_1}(z)h\right] \\ &\quad -\left[\tau_2'(z)h\right]\frac{\partial u_1}{\partial\tau}\circ z - \tau_2(z)\left[B'_{T,u_1}(z)h\right]. \end{aligned}$$

In summary, the linearized equation for IP2 is (44), where $G_N(z)$ and $G_N'(z)h$ are defined in (46) and (47), respectively.

4.2.3. Linearized Equation for IP3

For the inverse problem IP3, we denote the linearized equation by

$$G_R(z) + G_R'(z)h = 0 \tag{48}$$

for any approximation Γ to ∂D with parameterization $\Gamma := \{z(t), t\in[0,2\pi]\}$.

Since the total field u satisfies the Robin boundary condition:

$$2\mu\frac{\partial u}{\partial\nu} + \lambda\nu\,\mathrm{div}\, u + \mu\tau\,\mathrm{div}^{\perp} u + i\sigma u = 0$$

on the exact boundary ∂D, according to the definition of G in (38), the boundary operator for IP3 is

$$G_R(z) = 2\mu\frac{\partial u}{\partial\nu}\circ z + \lambda(\nu\,\mathrm{div}\, u)\circ z + \mu(\tau\,\mathrm{div}^{\perp} u)\circ z + i\sigma u\circ z. \tag{49}$$

From the definitions of G_D in (42) and G_N in (46), $G_R(z)$ can be rewritten as

$$G_R(z) = G_N(z) + i\sigma G_D(z). \tag{50}$$

Based on the Fréchet derivatives of G_D and G_N in (43) and (47), the Fréchet derivative of G_R is

$$G_R'(z)h = G_N'(z)h + i\sigma G_D'(z)h. \tag{51}$$

Therefore, the linearized equation for IP3 is (48), where $G_R(z)$ and $G'_R(z)h$ are defined in (50) and (51), respectively.

4.2.4. Linearized Equation for IP4

For the inverse problem IP4, we denote the linearized equation by

$$G_U(z) + G'_U(z)h = 0, \tag{52}$$

for any approximation Γ to ∂D with parameterization $\Gamma := \{z(t), t \in [0, 2\pi]\}$.

For the inverse problem IP4, the boundary condition of the object is unknown. However, according to Theorem 1, if the total field u satisfies the Dirichlet, Neumann, or Robin boundary condition on the exact boundary ∂D, then it satisfies the general boundary condition:

$$\begin{cases} \Re(T_\nu u). * \Re(u) + \Im(T_\nu u). * \Im(u) = 0 \\ \Re(T_\nu u). * \Re(u)^\perp + \Im(T_\nu u)^\perp . * \Im(u) = 0 \\ \Re(T_\nu u). * \Im(u)^\perp - \Re(T_\nu u)^\perp . * \Im(u) = 0 \\ \Im(T_\nu u). * \Re(u)^\perp - \Im(T_\nu u)^\perp . * \Re(u) = 0 \end{cases}$$

on ∂D. From the definition of G in (38), with the definitions of G_D in (42) and G_N in (46), the boundary operator G for IP4 is

$$G_U(z) = \begin{bmatrix} \Re(G_N(z)). * \Re(G_D(z)) + \Im(G_N(z)). * \Im(G_D(z)) \\ \Re(G_N(z)). * \Re(G_D(z))^\perp + \Im(G_N(z))^\perp . * \Im(G_D(z)) \\ \Re(G_N(z)). * \Im(G_D(z))^\perp - \Re(G_N(z))^\perp . * \Im(G_D(z)) \\ \Im(G_N(z)). * \Re(G_D(z))^\perp - \Im(G_N(z))^\perp . * \Re(G_D(z)) \end{bmatrix}. \tag{53}$$

By using the product rule, the Fréchet derivatives of G_D in (43), and the Fréchet derivatives of G_N in (47), we have

$$G'_U(z)h = \begin{bmatrix} \Re(G'_N(z)h). * \Re(G_D(z)) + \Re(G_N(z)). * \Re(G'_D(z)h) + \Im(G'_N(z)h). * \Im(G_D(z)) + \Im(G_N(z)). * \Im(G'_D(z)h) \\ \Re(G'_N(z)h). * \Re(G_D(z))^\perp + \Re(G_N(z)). * \Re(G'_D(z)h)^\perp + \Im(G'_N(z)h)^\perp . * \Im(G_D(z)) + \Im(G_N(z))^\perp . * \Im(G'_D(z)h) \\ \Re(G'_N(z)h). * \Im(G_D(z))^\perp + \Re(G_N(z)). * \Im(G'_D(z)h)^\perp - \Re(G'_N(z)h)^\perp . * \Im(G_D(z)) - \Re(G_N(z))^\perp . * \Im(G'_D(z)h) \\ \Im(G'_N(z)h). * \Re(G_D(z))^\perp + \Im(G_N(z)). * \Re(G'_D(z)h)^\perp - \Im(G'_N(z)h)^\perp . * \Re(G_D(z)) - \Im(G_N(z))^\perp . * \Re(G'_D(z)h) \end{bmatrix}$$

In summary, the linearized equation for IP4 is (52), where $G_U(z)$ is defined in (53) and $G'_U(z)h$ is given in the equation above.

5. Numerical Experiments

We present some numerical examples to show the performance of the proposed method. Three obstacles will be used: a triangle-shaped obstacle given by

$$(1 + 0.15\cos 3t)\big(\cos t,\ \sin t\big), \quad t \in [0, 2\pi],$$

a peanut-shaped obstacle given by

$$\sqrt{\cos^2 t + 0.25\sin^2 t}\big(\cos t,\ \sin t\big), \quad t \in [0, 2\pi],$$

and a kite-shaped obstacle given by

$$\big(-0.8\sin t - 0.4\cos 2t,\ 0.8\cos t\big), \quad t \in [0, 2\pi].$$

We set the parameters in the Navier equation to be $\omega = 3, \mu = 1, \lambda = 1$. In the case of the Robin boundary condition, we set $\sigma = 2$. The incident wave was set to be a plane wave $u^{inc}(x) = de^{ik_p x\cdot d} + d^{\perp}e^{ik_s x\cdot d}$ with incident direction $d = (0, -1)$. The synthetic far-field data $u_p^{\infty}(\hat{x}_j)$ and $u_s^{\infty}(\hat{x}_j)$ were generated at 128 equidistant points $\hat{x}_j, j = 1, 2, \ldots, 128$ on the unit circle by using the boundary integral method in [39] with 2% noise added.

The reconstructions are restricted to the star-shaped domain, that is the reconstructions $\Gamma_n, n = 1, 2, \ldots$ in the iterations have the parameterization:

$$z_n(t) = r_n(t)(\cos t, \sin t) + (c_1^{(n)}, c_2^{(n)}), \quad t \in [0, 2\pi].$$

where $r_n(t)$ is the radius function and $(c_1^{(n)}, c_2^{(n)})$ is the location. In our experiments, we used the radial function:

$$r_n(t) = a_0^{(n)} + \sum_{j=1}^{N} \left(a_j^{(n)} \cos jt + b_j^{(n)} \sin jt\right)$$

of degree $N = 5$.

We implemented the algorithm given in Section 4.1 to iteratively reconstruct the boundaries of the obstacles from the noisy far-field data. There are two steps in each iteration of the reconstruction algorithm. In the first step, we set $\tilde{\Gamma}_n$ to be a contraction of Γ_n with parameterization

$$\tilde{z}_n(t) = 0.9\, r_n(t)(\cos t, \sin t) + (c_1^{(n)}, c_2^{(n)}), \quad t \in [0, 2\pi].$$

Equations (36) and (37) were solved considering 128 points over the closed curve $\tilde{\Gamma}_n$. Then, the total field u, its normal derivative $\partial u/\partial \nu$, and its tangential derivative $\partial u/\partial \tau$ can be computed at 128 discrete points on Γ_n using the discrete form of (35). In the second step, since the shift function $h(t)$ has the same form as $z_n(t)$,

$$h(t) = \left[a_0^{(h)} + \sum_{j=1}^{N} \left(a_j^{(h)} \cos jt + b_j^{(h)} \sin jt\right)\right](\cos t, \sin t) + (c_1^{(h)}, c_2^{(h)}), \quad t \in [0, 2\pi],$$

the linearized Equation (39) can be discretized into a linear system of $2N + 3$ real variables $a_0^{(h)}$, $c_1^{(h)}$, $c_2^{(h)}$, and $a_j^{(h)}, b_j^{(h)}, j = 1, 2, \ldots, N$. One should consider both the real part and imaginary parts of the linear system to obtain real solutions. In the computation of the discrete system of (39), if $\partial^2 u/\partial \nu^2$, $\partial^2 u/\partial \tau^2$, and $\partial^2 u/\partial \tau \partial \nu$ occur in the expressions of G', one can use the difference method or the second derivatives of (35) to solve them. Our experiments used the difference method to solve $\partial^2 u/\partial \nu^2$, $\partial^2 u/\partial \tau^2$, and $\partial^2 u/\partial \tau \partial \nu$ based on $\partial u/\partial \nu$ and $\partial u/\partial \tau$. Tikhonov regularization was used in the solution of (36) and (37) and in the solution of the linearized Equation (39), and the regularization parameters were determined by the L-curve method [40].

In the following figures, the blue solid lines are the exact boundaries, the red dashed lines are the reconstructions, and the black dotted lines are the initial guesses of the boundaries.

5.1. Examples for IP1

For the inverse problem IP1, the Dirichlet boundary condition is known to be satisfied on the exact boundary of the obstacle. The hybrid method for IP1 is used in this subsection, that is the linearized Equation (40) was used in the algorithm.

Figure 1 displays reconstructions of the rigid triangle: The left panel shows the reconstruction result, and the initial guess is a circle with radius 0.5 centered at $(-0.1, 0.2)$. The right panel is the plot of $\|u\|_{L^2(\Gamma_n)}$ against the number of iterations n. We can see that the Dirichlet boundary condition is satisfied increasingly well on the n-th approximation Γ_n

as n increases. Similar reconstruction results for the rigid peanut and rigid kite are shown in Figure 2.

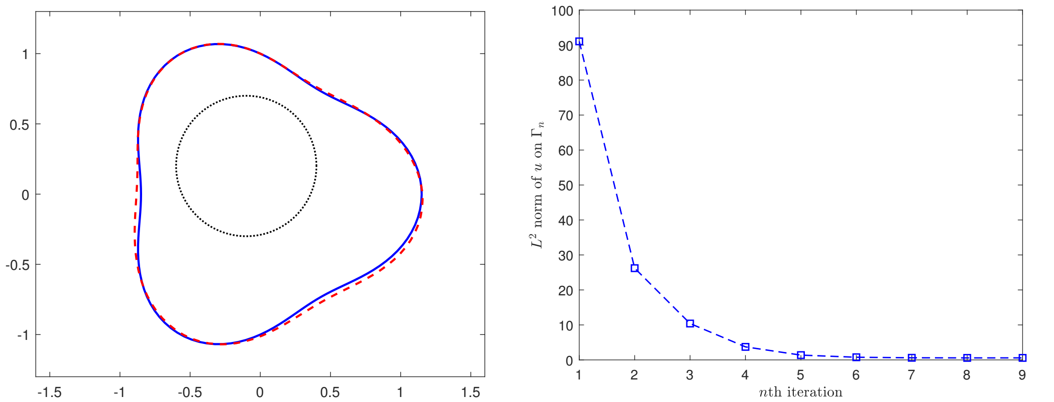

Figure 1. Reconstruction of the triangle with Dirichlet BC by the hybrid method for IP1. **Left**: reconstruction result after 9 iterations. **Right**: plot of $\|u\|_{L^2(\Gamma_n)}$ against the number of iterations n.

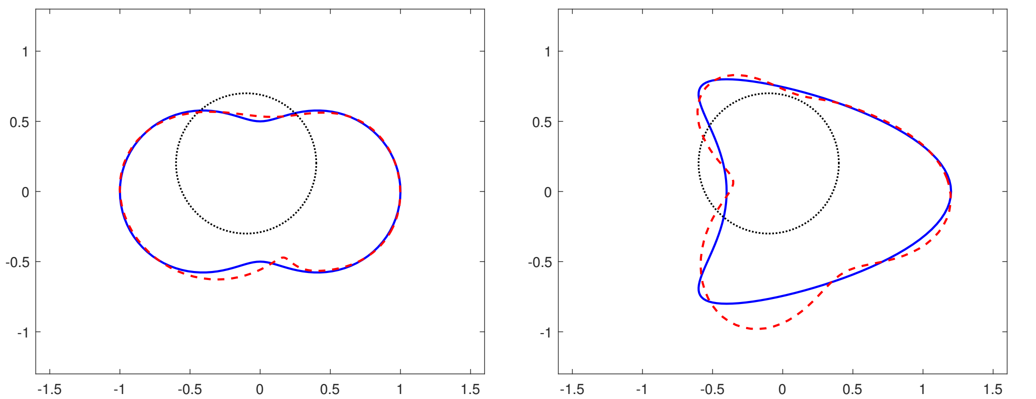

Figure 2. Reconstructions of the peanut and the kite with Dirichlet BC by the hybrid method for IP1. **Left**: reconstruction result for the rigid peanut after 50 iterations. **Right**: reconstruction result for the rigid kite after 13 iterations.

5.2. Examples for IP2

For the inverse problem IP2, the Neumann boundary condition is known to be satisfied on the exact boundary of the obstacle. The hybrid method for IP2 is used in this subsection, that is the linearized Equation (44) was used in the algorithm.

Figure 3 displays the reconstructions of the cavity triangle. The left panel shows the reconstruction result when the initial guess is a circle with radius 0.5 centered at $(-0.1, 0.2)$; the right panel is the plot of $\|T_\nu u\|_{L^2(\Gamma_n)}$ against the number of iterations n. We can see that the Neumann boundary condition is satisfied increasingly well on Γ_n as the iteration number n increases. Similar reconstruction results for the cavity peanut and cavity kite are shown in Figure 4.

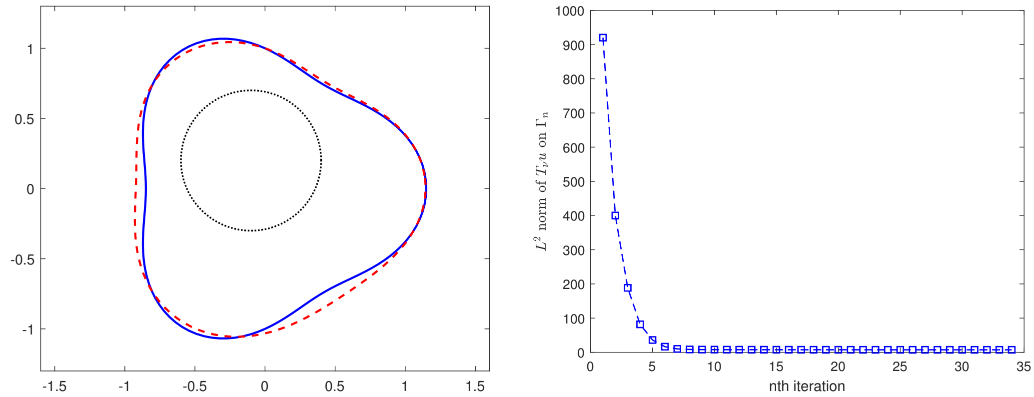

Figure 3. Reconstruction of the triangle with Neumann BC by the hybrid method for IP2. **Left**: reconstruction result after 34 iterations. **Right**: plot of $\|T_\nu u\|_{L^2(\Gamma_n)}$ against the number of iterations n.

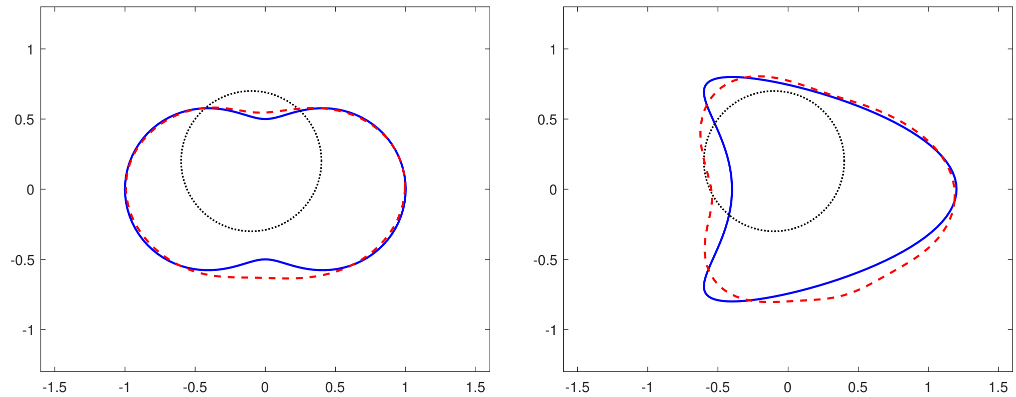

Figure 4. Reconstructions of the peanut and the kite with Neumann BCs by the hybrid method for IP2. **Left**: reconstruction result for the peanut after 50 iterations. **Right**: reconstruction result for the kite after 24 iterations.

5.3. Examples for IP3

For the inverse problem IP3, the Robin boundary condition is known to be satisfied on the exact boundary of the obstacle. The hybrid method for IP3 is used in this subsection, that is the linearized Equation (48) is used in the algorithm.

Figure 5 displays reconstructions of the triangle with the Robin boundary condition: The left panel shows the reconstruction result when the initial guess is a circle with radius 0.5 centered at $(-0.1, 0.2)$. The right panel is the plot of $\|T_\nu u + i\sigma u\|_{L^2(\Gamma_n)}$ against the number of iterations n. We can see that the Robin boundary condition is increasingly satisfied on the n-th approximation Γ_n as n increases. Similar reconstruction results for the peanut-shaped obstacle with the Robin boundary condition and the kite-shaped obstacle with the Robin boundary condition are shown in Figure 6.

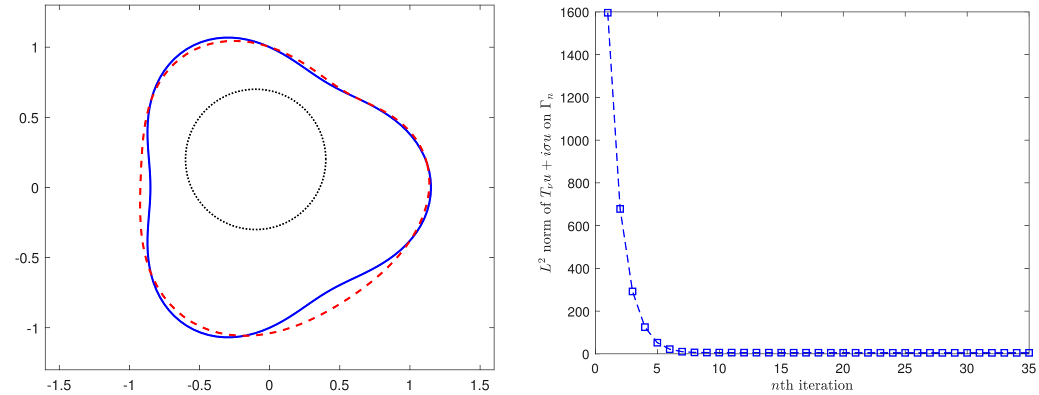

Figure 5. Reconstructions of the triangle with Robin BC by the hybrid method for IP3. **Left**: reconstruction result after 35 iterations. **Right**: plot of $\|T_\nu u + i\sigma u\|_{L^2(\Gamma_n)}$ against the number of iterations n.

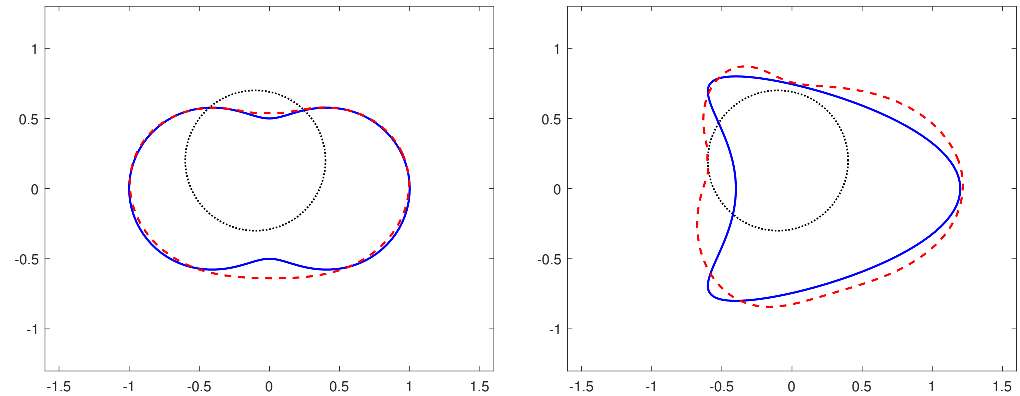

Figure 6. Reconstructions of the peanut and kite with Robin BCs by the hybrid method for IP3. **Left**: reconstruction result for the peanut after 20 iterations. **Right**: reconstruction result for the kite after 20 iterations.

5.4. Examples for IP4

For the inverse problem IP4, the boundary condition is unknown, and the hybrid method for IP4 is based on the artificial general boundary condition (8). For all the experiments in this subsection, the boundary conditions of the obstacles were not used in the reconstruction algorithm; they were only used in the generation of the synthetic far-field data.

Figure 7 displays reconstructions of the triangle-shaped obstacle with the Dirichlet boundary condition: the left panel shows the reconstruction result when the initial guess is a circle with radius 0.5 centered at $(-0.1, 0.2)$; the right panel is the plot of $\|G_U(z_n)\|_{L^2}$ against the number of iterations n. We can see that the artificial boundary condition is increasingly satisfied on the n-th approximation Γ_n as n increases. Similar reconstructions for the peanut with the Neumann boundary condition and kite with the Robin boundary condition are shown in Figures 8 and 9, respectively. Figure 10 shows the reconstruction results for these three obstacles with the other two boundary conditions.

The hybrid iterative method also works with different initial guesses and different incident waves. Figure 11 shows the reconstruction results when we changed the initial guess to be $B_{0.8}(0,0)$, which is a circle with radius 0.8 centered at the origin. Figure 12 shows the reconstruction results when we changed the incident direction to $(1, 0)$.

For the case of an acoustic wave, a local convergence result for the hybrid method was established in [31]. For the case of an elastic wave, we can also observe the local convergence of the hybrid method from Figures 1, 3, 5, and 7–9.

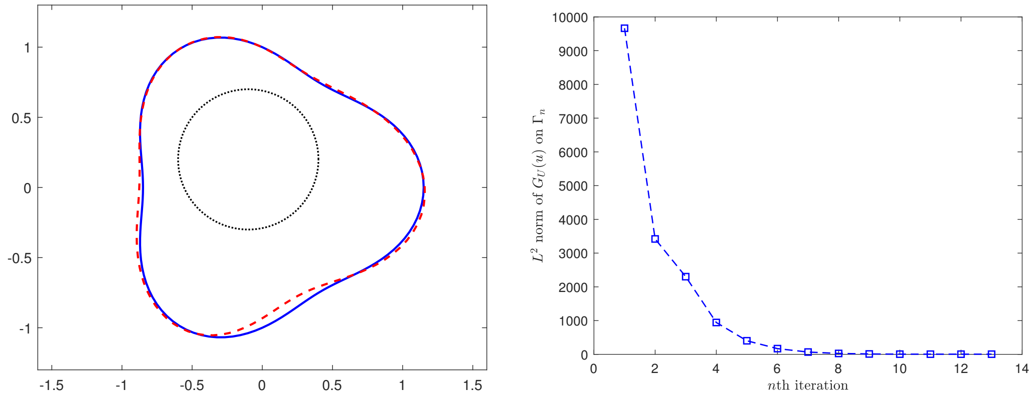

Figure 7. Reconstructions of the triangle with Dirichlet BC by the hybrid method for IP4. **Left**: reconstruction result after 13 iterations. **Right**: plot of $\|G_U(u)\|_{L^2(\Gamma_n)}$ against the number of iterations n.

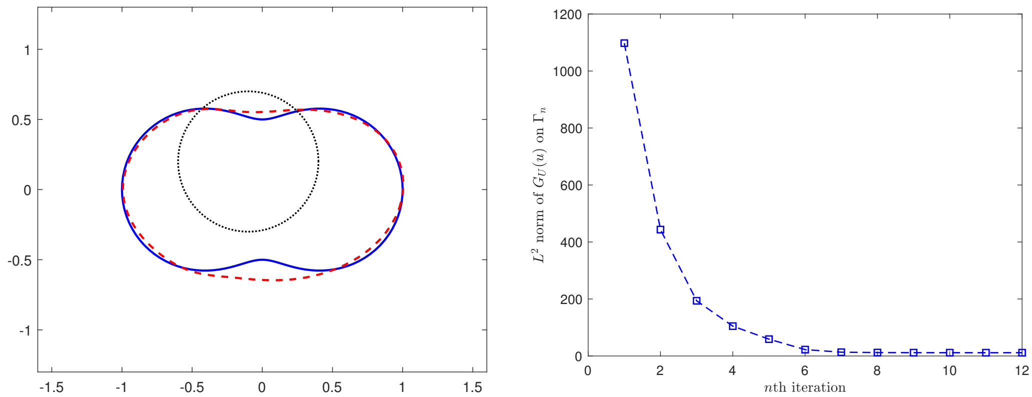

Figure 8. Reconstructions of the peanut with Neumann BC by the hybrid method for IP4. **Left**: reconstruction result after 12 iterations. **Right**: plot of $\|G_U(u)\|_{L^2(\Gamma_n)}$ against the number of iterations n.

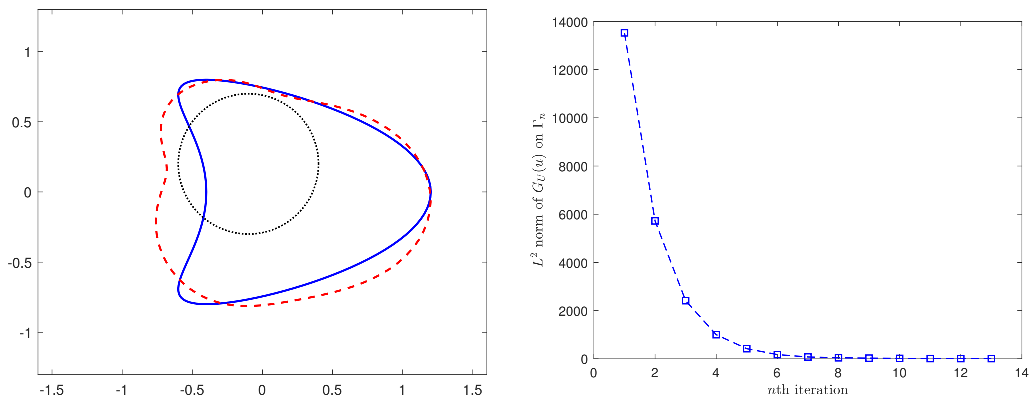

Figure 9. Reconstructions of the kite with Robin BC by the hybrid method for IP4. **Left**: reconstruction result after 13 iterations. **Right**: plot of $\|G_U(u)\|_{L^2(\Gamma_n)}$ against the number of iterations n.

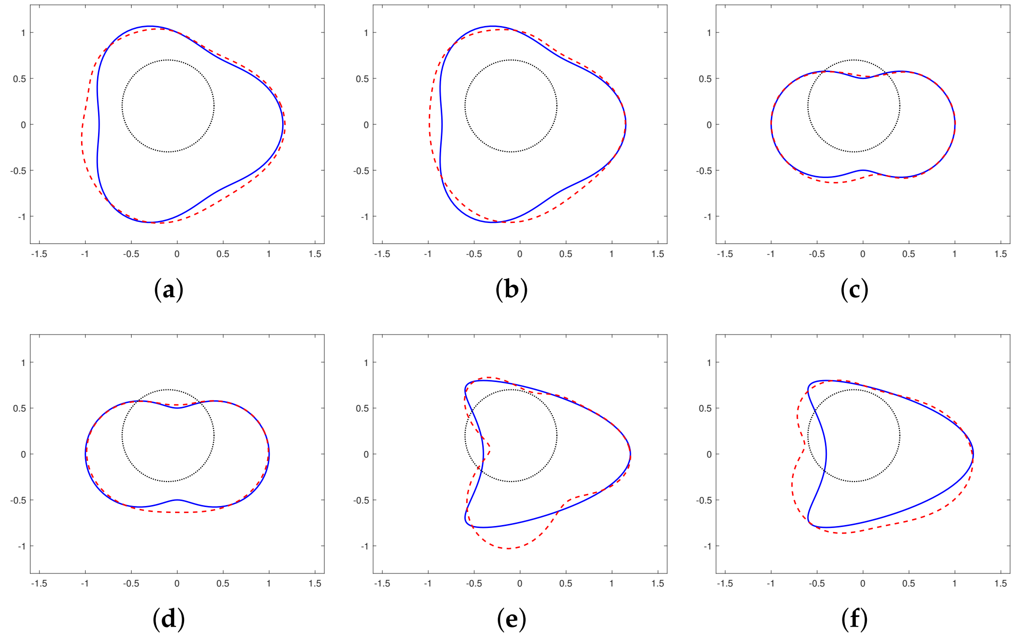

Figure 10. Reconstruction results of three obstacles with different boundary conditions by the hybrid method for IP4: (**a**) reconstruction of the triangle with Neumann BC after 14 iterations; (**b**) reconstruction of the triangle with Robin BC after 16 iterations; (**c**) reconstruction of the peanut with Dirichlet BC after 24 iterations; (**d**) reconstruction of the peanut with Robin BC after 37 iterations; (**e**) reconstruction of the kite with Dirichlet BC after 15 iterations; (**f**) reconstruction of the kite with Neumann BC after 13 iterations.

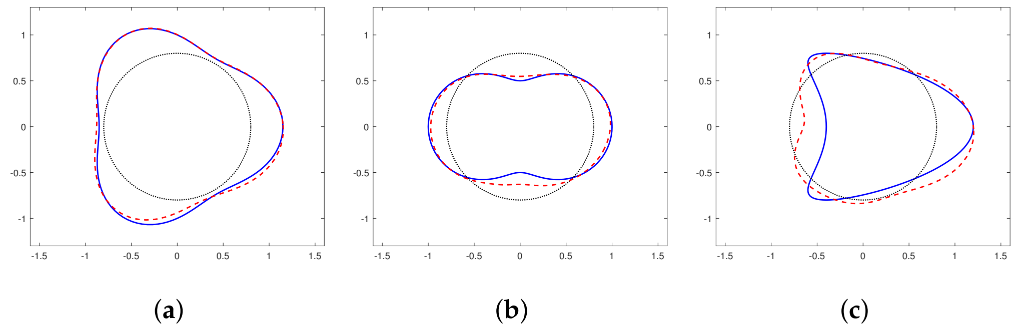

Figure 11. Reconstruction results by the hybrid method for IP4 with the initial guess $B_{0.8}(0,0)$: (**a**) reconstruction of the triangle with Dirichlet BC after 8 iterations; (**b**) reconstruction of the peanut with Neumann BC after 9 iterations; (**c**) reconstruction of the kite with Robin BC after 7 iterations.

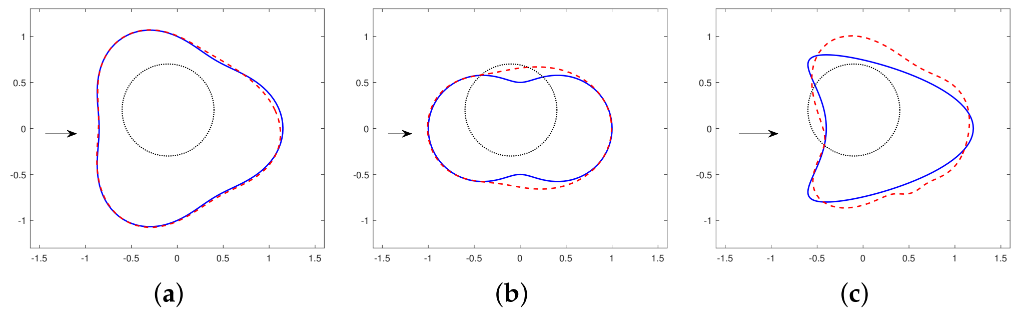

Figure 12. Reconstruction results by the hybrid method for IP4 with the incident direction $(1,0)$: (**a**) reconstruction of the triangle with Dirichlet BC after 18 iterations; (**b**) reconstruction of the peanut with Neumann BC after 13 iterations; (**c**) reconstruction of the kite with Robin BC after 30 iterations.

6. Conclusions

In this paper, we considered four inverse elastic scattering problems of reconstructing obstacles using the far-field of a single incident wave. For the first three inverse elastic scattering problems, the boundary conditions of the obstacles are available. By introducing Fréchet derivatives of the tangential operator and tangential derivative operator, we extended the hybrid method for inverse acoustic scattering problems to the case of inverse elastic scattering problems. For the fourth inverse elastic scattering problem with the boundary condition unknown, by introducing a general boundary condition and analyzing the equivalence of the general boundary condition and three commonly used boundary conditions, we extended the hybrid method to solve the fourth inverse elastic scattering problem.

As far as we know, the existing iterative methods for inverse elastic obstacle scattering problems require forward solvers and, therefore, need the boundary condition of the obstacle. In this paper, we established an iterative method that can reconstruct obstacles with or without known boundary conditions. This is significant because one can determine the shapes of obstacles even when the physical properties of the obstacles are not available. The numerical experiments showed the efficiency of the method.

In the future, with the theoretical results regarding the boundary conditions and Fréchet derivatives of the boundary operators, we hope to propose iterative methods for more inverse obstacle problems with complicated boundary conditions.

Author Contributions: Methodology, J.L.; software, Y.Y.; writing—original draft, Y.Y.; writing—review and editing, J.L. All authors have read and agreed to the published version of the manuscript.

Funding: This research was funded by the NSF of China under Grant No. 11801218.

Data Availability Statement: The data presented in this study are available on request from the corresponding author. The data are not publicly available due to privacy.

Conflicts of Interest: The authors declare no conflict of interest.

References

1. Colton, D.L.; Kress, R. *Inverse Acoustic and Electromagnetic Scattering Theory*; Springer: Berlin/Heidelberg, Germany, 1998; Volume 93.
2. Ji, X.; Liu, X.; Xi, Y. Direct sampling methods for inverse elastic scattering problems. *Inverse Probl.* **2018**, *34*, 035008. [CrossRef]
3. Ji, X.; Liu, X. Inverse elastic scattering problems with phaseless far-field data. *Inverse Probl.* **2019**, *35*, 114004. [CrossRef]
4. Ma, G.; Hu, G. Factorization method with one plane wave: from model-driven and data-driven perspectives. *Inverse Probl.* **2021**, *38*, 015003. [CrossRef]
5. Hu, G.; Mantile, A.; Sini, M.; Yin, T. Direct and Inverse Time-Harmonic Elastic Scattering from Point-Like and Extended Obstacles. *Inverse Probl. Imaging* **2020**, *14*, 1025–1056. [CrossRef]
6. Ma, G.; Hu, G. Factorization method for inverse time-harmonic elastic scattering with a single plane wave. *Discret. Contin. Dyn. Syst.-B* **2022**, *27*, 7469–7492. [CrossRef]
7. Meng, Q.; Bai, Z.; Diao, H.; Liu, H. Effective medium theory for embedded obstacles in elasticity with applications to inverse problems. *SIAM J. Appl. Math.* **2022**, *82*, 720–749. [CrossRef]
8. Dong, H.; Lai, J.; Li, P. Inverse obstacle scattering for elastic waves with phased or phaseless far-field data. *SIAM J. Imaging Sci.* **2019**, *12*, 809–838. [CrossRef]
9. Kupradze, V.D.; Gegelia, T.G.; Basheleishvili, M.O.; Burchuladze, T.V. Three-Dimensional Problems of the Mathematical Theory of Elasticity and Thermoelasticity. *Appl. Mech. ASME J.* **1979**. [CrossRef]
10. Bonnet, M.; Constantinescu, A. Inverse problems in elasticity. *Inverse Probl.* **2005**, *21*, R1. [CrossRef]
11. Lurie, A.I. *Theory Elast*; Springer: Berlin/Heidelberg, Germany, 2010.
12. Ammari, H.; Bretin, E.; Garnier, J.; Kang, H.; Lee, H.; Wahab, A. *Mathematical Methods in Elasticity Imaging*; Princeton University Press: Princeton, NJ, USA, 2015; Volume 52.
13. Arens, T. Linear sampling methods for 2D inverse elastic wave scattering. *Inverse Probl.* **2001**, *17*, 1445. [CrossRef]
14. Alves, C.J.; Kress, R. On the far-field operator in elastic obstacle scattering. *IMA J. Appl. Math.* **2002**, *67*, 1–21. [CrossRef]
15. Hu, G.; Kirsch, A.; Sini, M. Some inverse problems arising from elastic scattering by rigid obstacles. *Inverse Probl.* **2012**, *29*, 015009. [CrossRef]
16. Xiang, J.; Yan, G. The factorization method for a mixed inverse elastic scattering problem. *IMA J. Appl. Math.* **2022**, *87*, 407–437. [CrossRef]

17. Chen, Z.; Huang, G. Reverse time migration for extended obstacles: Elastic waves. *Sci. China Math.* **2015**, *45*, 1103–1114. (In Chinese)
18. Liu, J.; Liu, X.; Sun, J. Extended sampling method for inverse elastic scattering problems using one incident wave. *SIAM J. Imaging Sci.* **2019**, *12*, 874–892. [CrossRef]
19. Liu, J.; Sun, J. Extended sampling method in inverse scattering. *Inverse Probl.* **2018**, *34*, 085007. [CrossRef]
20. Elschner, J.; Hu, G. Uniqueness and factorization method for inverse elastic scattering with a single incoming wave. *Inverse Probl.* **2019**, *35*, 094002. [CrossRef]
21. Li, P.; Wang, Y.; Wang, Z.; Zhao, Y. Inverse obstacle scattering for elastic waves. *Inverse Probl.* **2016**, *32*, 115018. [CrossRef]
22. Bao, G.; Hu, G.; Sun, J.; Yin, T. Direct and inverse elastic scattering from anisotropic media. *J. Mathématiques Pures Appliquées* **2018**, *117*, 263–301. [CrossRef]
23. Li, P.; Yuan, X. Inverse obstacle scattering for elastic waves in three dimensions. *Inverse Probl. Imaging* **2019**, *13*, 545–573. [CrossRef]
24. Li, Z.; Sun, J.; Xu, L. An extended sampling-ensemble Kalman filter approach for partial data inverse elastic problems. *Inverse Probl. Sci. Eng.* **2021**, *29*, 2534–2550. [CrossRef]
25. Elschner, J.; Yamamoto, M. Uniqueness in inverse elastic scattering with finitely many incident waves. *Inverse Probl.* **2010**, *26*, 045005. [CrossRef]
26. Chapko, R.; Kress, R. A hybrid method for inverse boundary value problems in potential theory. *J. Inverse Ill-Posed Probl.* **2005**, *13*, 27–40. [CrossRef]
27. Kress, R.; Serranho, P. A hybrid method for two-dimensional crack reconstruction. *Inverse Probl.* **2005**, *21*, 773. [CrossRef]
28. Kress, R.; Serranho, P. A hybrid method for sound-hard obstacle reconstruction. *J. Comput. Appl. Math.* **2007**, *204*, 418–427. [CrossRef]
29. Serranho, P. A hybrid method for inverse scattering for shape and impedance. *Inverse Probl.* **2006**, *22*, 663. [CrossRef]
30. Serranho, P. A hybrid method for inverse scattering for sound-soft obstacles in R3. *Inverse Probl. Imaging* **2007**, *1*, 691. [CrossRef]
31. Serranho, P. A Hybrid Method for Inverse Obstacle Scattering Problems. Ph.D Thesis, Georg-August-Universität Göttingen: Göttingen, Germany, 2007.
32. Kirsch, A.; Kress, R. On an integral equation of the first kind in inverse acoustic scattering. In *Inverse Problems*; Springer: Berlin/Heidelberg, Germany, 1986; pp. 93–102.
33. Kirsch, A.; Kress, R. A numerical method for an inverse scattering problem. In *Inverse and Ill-Posed Problems*; Elsevier: Amsterdam, The Netherlands, 1987; pp. 279–289.
34. Elschner, J.; Hsiao, G.C.; Rathsfeld, A. An optimization method in inverse acoustic scattering by an elastic obstacle. *SIAM J. Appl. Math.* **2009**, *70*, 168–187. [CrossRef]
35. Kress, R.; Rundell, W. Nonlinear integral equations and the iterative solution for an inverse boundary value problem. *Inverse Probl.* **2005**, *21*, 1207. [CrossRef]
36. Ivanyshyn, O.; Kress, R. Nonlinear integral equations for solving inverse boundary value problems for inclusions and cracks. *J. Integral Equ. Appl.* **2006**, *18*, 13–38. [CrossRef]
37. Liu, J.; Fuming, M. An Improved Hybrid Method for Inverse Obstacle Scattering Problems. *Commun. Math. Res.* **2011**, *27*, 215–226.
38. Vinogradov, S.S.; Smith, P.D.; Vinogradova, E.D. *Canonical Problems in Scattering and Potential Theory Part II: Acoustic and Electromagnetic Diffraction by Canonical Structures*; CRC: Boca Raton, FL, USA, 2002.
39. Kress, R. Inverse elastic scattering from a crack. *Inverse Probl.* **1996**, *12*, 667. [CrossRef]
40. Hansen, P.C. Regularization tools: A Matlab package for analysis and solution of discrete ill-posed problems. *Numer. Algorithms* **1994**, *6*, 1–35. [CrossRef]